

RESEARCH

Open Access



NEAT1 regulates BMSCs aging through disruption of FGF2 nuclear transport

Zifei Wang^{1†}, Wenyu Zhen^{1†}, Qing Wang^{1†}, Yuqiang Sun^{1†}, Siyu Jin¹, Sensen Yu¹, Xing Wu¹, Wenhao Zhang¹, Yulong Zhang¹, Fei Xu¹, Rui Wang¹, Yuxuan Xie¹, Wansu Sun^{2*}, Jianguang Xu^{1*} and Hengguo Zhang^{1*} 

Abstract

Background The aging of bone marrow mesenchymal stem cells (BMSCs) impairs bone tissue regeneration, contributing to skeletal disorders. LncRNA NEAT1 is considered as a proliferative inhibitory role during cellular senescence, but the relevant mechanisms remain insufficient. This study aims to elucidate how NEAT1 regulates mitotic proteins during BMSCs aging.

Methods BMSCs were isolated from alveolar bone of human volunteers aged 26–33 (young) and 66–78 (aged). NEAT1 expression and distribution changes during aging process were observed using fluorescence in situ hybridization (FISH) in young (3 months) and aged (18 months) mice or human BMSCs. Subsequent RNA pulldown and proteomic analyses, along with single-cell analysis, immunofluorescence, RNA immunoprecipitation (RIP), and co-immunoprecipitation (Co-IP), were conducted to investigate that NEAT1 impairs the nuclear transport of mitotic FGF2 and contributes to BMSCs aging.

Results We reveal that NEAT1 undergoes significant upregulated and shifts from nucleus to cytoplasm in bone marrow and BMSCs during aging process. In which, the expression correlates with nuclear DNA content during karyokinesis, suggesting a link to mitogenic factor. Within NEAT1 knockdown, hallmarks of cellular aging, including senescence-associated secretory phenotype (SASP), p16, and p21, were significantly downregulated. RNA pulldown and proteomic analyses further identify NEAT1 involved in osteoblast differentiation, mitotic cell cycle, and ribosome biogenesis, highlighting its role in maintaining BMSCs differentiation and proliferation. Notably, as an essential growth factor of BMSCs, Fibroblast Growth Factor 2 (FGF2) directly abundant binds to NEAT1 and the sites enriched with nuclear localization motifs. Importantly, NEAT1 decreased the interaction between FGF2 and Karyopherin Subunit Beta 1 (KPNB1), influencing the nuclear transport of mitogenic FGF2.

[†]Zifei Wang, Wenyu Zhen, Qing Wang and Yuqiang Sun contributed equally to this work.

*Correspondence:

Wansu Sun
sunwansu@ahmu.edu.cn
Jianguang Xu
xujianguang@ahmu.edu.cn
Hengguo Zhang
zhanghengguo@ahmu.edu.cn

Full list of author information is available at the end of the article



© The Author(s) 2025. **Open Access** This article is licensed under a Creative Commons Attribution-NonCommercial-NoDerivatives 4.0 International License, which permits any non-commercial use, sharing, distribution and reproduction in any medium or format, as long as you give appropriate credit to the original author(s) and the source, provide a link to the Creative Commons licence, and indicate if you modified the licensed material. You do not have permission under this licence to share adapted material derived from this article or parts of it. The images or other third party material in this article are included in the article's Creative Commons licence, unless indicated otherwise in a credit line to the material. If material is not included in the article's Creative Commons licence and your intended use is not permitted by statutory regulation or exceeds the permitted use, you will need to obtain permission directly from the copyright holder. To view a copy of this licence, visit <http://creativecommons.org/licenses/by-nc-nd/4.0/>.

Conclusions Our findings position NEAT1 as a critical regulator of mitogenic protein networks that govern BMSC aging. Targeting NEAT1 might offer novel therapeutic strategies to rejuvenate aged BMSCs.

Introduction

Aging is a complex biological process marked by the progressive decline in physiological functions and regenerative capacity [1]. At the cellular level, aging manifests as widespread alterations in gene expression, protein interactions, and subcellular organization, ultimately leading to impaired cell cycle regulation and homeostasis [2, 3]. During the aging process, aged bone marrow mesenchymal stem cells (BMSCs) is characterized by cell cycle arrest and a notable reduction in their capacity for osteoblast differentiation, making the replacement and repair of bone tissue increasingly difficult [4, 5]. The diminished regenerative potential of aged BMSCs contributes directly to the onset of skeletal disorders, such as osteoporosis and impaired fracture healing [6, 7]. These age-related dysfunctions in BMSC activity underscore the need for a deeper understanding of the molecular drivers of cellular senescence and tissue regeneration.

Long non-coding RNAs (lncRNAs), a class of RNA molecules exceeding 200 nucleotides in length, have recently emerged as pivotal regulators of gene expression and cellular functions [8]. lncRNAs exert their influence through various mechanisms, including chromatin remodeling, transcriptional regulation, and post-transcriptional modifications [9, 10]. Among them, Nuclear Paraspeckle Assembly Transcript 1 (NEAT1) has received significant attention due to its role in the formation and maintenance of paraspeckle nuclear bodies, which is involved in gene regulation, RNA processing, and cellular stress responses [11, 12]. NEAT1 exists in two isoforms: the shorter NEAT1_1 (3.7 kb) and the longer NEAT1_2 (23 kb) [13, 14]. While extensive research has highlighted NEAT1's contribution to nuclear architecture, paraspeckle assembly, and DNA repair pathways under oxidative stress, its role in the aging of BMSCs and their ability in bone regeneration remains insufficiently explored [15–17].

Fibroblast Growth Factor 2 (FGF2), a critical mitogen for BMSCs, plays a key role in several physiological processes, including angiogenesis, wound healing, and osteogenesis [18–20]. FGF2's mitogenic properties are particularly relevant in the context of BMSC function, where it supports proliferation and differentiation [21–23]. Additionally, Karyopherin Subunit Beta 1 (KPNB1), a nuclear transport protein, is essential for the translocation of proteins and ribonucleoproteins across the nuclear envelope [24, 25]. The precise coordination between FGF2, KPNB1, and other mitogenic proteins is essential for maintaining cellular function and supporting tissue regeneration [26]. Disruption in these protein

interactions could lead to compromised cell function and contribute to the age-related decline in regenerative potential seen in BMSCs [27].

In this study, we propose that NEAT1 plays a critical role in regulating BMSC aging and bone regeneration by modulating the interactions between key mitogenic proteins, particularly FGF2 and KPNB1. We hypothesize that NEAT1 exerts its regulatory influence by altering itself subcellular localization and attenuating the interactions of these proteins, thereby affecting the regenerative capacity of BMSCs. Using a multifaceted approach, including NEAT1 fluorescence in situ hybridization (FISH), NEAT1 pulldown, proteomics analysis, and single-cell analysis, we aim to elucidate how NEAT1 shapes the mitogenic protein network and contributes to the aging of BMSCs. By understanding how NEAT1 orchestrates the interaction between mitogenic proteins such as FGF2 and KPNB1 may open new avenues for the treatment of age-associated bone diseases, thereby contributing to the broader field of regenerative medicine and aging research.

Materials and methods

Animals

The work has been reported in line with the ARRIVE guidelines 2.0. All animal experimental procedures were approved by the Laboratory Animal Care and Use Committee at Anhui Medical University (Approval No. LLSC20220738). Three-month-old and eighteen-month-old C57BL/6 mice were representing young and aged mice, respectively. After anesthetized with 2% sodium pentobarbital (50 mg/kg, intraperitoneal), mice were immobilized and subjected to the alveolar bone healing model (extract the first molar). Sample sizes and inclusion criteria were determined to ensure adequate statistical power, guided by existing literature and prior experience [15]. Mice were euthanized via rapid CO₂ asphyxiation followed by cervical dislocation, and alveolar bone tissues were harvested for histological analyses.

Primary cell culture

BMSCs were isolated from human alveolar bone specimens obtained from volunteers aged 26–33 (young) and 66–78 (aged), all of whom provided informed consent. Inclusion criteria and cell culture protocols adhered to established methods as described previously [15]. All procedures involving human MSCs were approved by the Ethical Committee at the College & Hospital of Stomatology of Anhui Medical University (Approval No. T2021014). BMSCs were cultured in Gibco™ BASIC

MEM α medium (Thermo Fisher Scientific) supplemented with 10% fetal bovine serum (ScienCell) and 1% penicillin-streptomycin, maintained at 37 °C in a humidified atmosphere with 5% CO₂.

To evaluate the distinct characteristics of BMSCs from human alveolar bone specimens, flow cytometry analysis showed that the isolated cells were negative for CD45 (0.24%), CD34 (1.11%), and CD11b (0.25%), surface markers of BMSCs, and positive for CD44 (99.97%), CD105 (91.25%), CD29 (99.96%), and CD73 (99.83%) (Figure S1a-A). The BMSCs exhibited a typical spindle-shaped morphology, with cells growing in a spindle-like or irregular triangular shape on the surface of the culture substrate (Figure S1a-B). We next assessed differentiation potential of the BMSCs, we induced osteogenic and adipogenic differentiation of BMSCs in vitro. After 21 days, staining with alizarin red and oil red O revealed clear mineralized nodules in the osteogenic group and distinct lipid droplets in the adipogenic group, thereby confirming the multilineage differentiation potential of the isolated BMSCs (Figure S1a-C).

Transfection of small interfering RNAs (siRNAs) and plasmids

siRNAs targeting NEAT1 was designed and synthesized by RiboBio (Guangzhou, China). An adenoviral vector GV315 containing NEAT1 (NR_028272) were purchased from GeneChem Co. (Shanghai, China). Transfections were performed using Lipofectamine 2000 (Invitrogen) according to the manufacturer's instructions. All sequence details are provided in Supplementary Table 1.

Cell senescence-associated β -galactosidase (SA- β -gal) staining

BMSCs were seeded in 12-well plates and incubated with staining solution according to the SA- β -gal kit (GENMED, Shanghai, China). After 16 h of coculture, five randomly selected fields were chosen to quantify SA β -gal positive cells under inverted microscopy.

Fluorescence in situ hybridization (FISH)

Fluorescence in situ hybridization probes were custom-designed and synthesized by RiboBio. The subcellular localization of NEAT1 in BMSCs was assessed using a FISH kit (RiboBio). Briefly, BMSCs seeded on coverslips and frozen femur sections were fixed with 4% paraformaldehyde for 15 min at 4 °C and permeabilized with 1% Triton X-100 for 20 min. Coverslips were incubated in prehybridization buffer at 37 °C for 30 min, followed by overnight hybridization at 37 °C in the dark with probes. Post-hybridization washes were conducted with decreasing concentrations of SSC buffer at 42 °C. Nuclei were counterstained with DAPI for 10 min, and samples were visualized using confocal fluorescence microscopy.

RNA pull-down

LncRNA NEAT1 pull-down assays were performed using the Pierce™ Magnetic RNA-Protein Pull-Down Kit (#20164, Thermo Fisher Scientific) per the manufacturer's protocol. Biotin-labeled oligonucleotide probes targeting junction sites of sense and antisense NEAT1 (NR_028272) were synthesized by GenePharma. Undifferentiated BMSCs (1×10^7 cells) were lysed in IP lysis buffer (#87787, Thermo Fisher Scientific) supplemented with protease and RNase inhibitors. Probes were incubated with streptavidin magnetic beads, and RNA-protein complexes were isolated. Eluted proteins were analyzed via silver staining, mass spectrometry, and Western blotting. RNA was extracted using TRIzol reagent for further analysis. Detailed probe sequences and antibody information are listed in Supplementary Table 1.

LC-MS/MS analysis

Protein digestion was carried out using the Filter-Aided Sample Preparation (FASP) protocol. Briefly, detergents, DTT, and low-molecular-weight contaminants were removed by ultrafiltration with 200 μ L of UA buffer (8 M urea, 150 mM Tris-HCl, pH 8.0) using 10 kDa Microcon filters under centrifugal concentration. For cysteine residue blocking, 100 μ L of 0.05 M iodoacetamide in UA buffer was added, and the samples were incubated in the dark for 20 min. The filters were washed with 100 μ L of UA buffer three times, followed by two washes with 100 μ L of 25 mM NH₄HCO₃. Protein digestion occurred overnight at 37 °C with 3 μ g trypsin (Promega) in 40 μ L of 25 mM NH₄HCO₃, and the peptides were collected in the filtrate.

LC-MS/MS analysis was performed on a Q Exactive HF-X mass spectrometer coupled with an Easy nLC system (Thermo Fisher Scientific). The peptide mixture was loaded onto an in-house packed C18 reversed-phase column (15 cm \times 75 μ m, 5 μ m resin) equilibrated with buffer A (0.1% formic acid in HPLC-grade water). Peptides were separated using a linear gradient of buffer B (0.1% formic acid in 84% acetonitrile) at 250 nL/min for 60 min, controlled by IntelliFlow technology. Data were acquired in a data-dependent top-10 mode, dynamically selecting the most abundant precursor ions (300–1800 m/z) for HCD fragmentation. Target values were set by predictive Automatic Gain Control (pAGC), and dynamic exclusion was applied for 20 s. Survey scans were obtained at a resolution of 70,000 at m/z 200, while HCD spectra were recorded at a resolution of 17,500 at m/z 200. Normalized collision energy was set to 27 eV, and the underfill ratio (the minimal percentage of the target value likely to be reached at maximum fill time) was set to 0.1%. MS data were processed with MaxQuant software (version 1.3.0.5). The data were searched against the UniProtKB

Homo sapiens database (194,237 entries, downloaded 2020-12-10). The search included a precursor mass window of 6 ppm and allowed up to two missed cleavages by trypsin, with a fragment ion mass tolerance of 20 ppm. Carbamidomethylation of cysteine (C) was defined as a fixed modification, and oxidation of methionine (M) and phosphorylation of serine, threonine, and tyrosine (S/T/Y) were defined as variable modifications. A false discovery rate (FDR) of 0.01 was applied for peptide and protein identification.

Analysis of single-cell RNA-Seq and RNA-Seq

Single-cell RNA-seq data from 2,221 telomerase-immortalized human BMSCs were obtained from NCBI GEO (GSM3439738). Quality control and normalization were conducted using Seurat. Highly variable genes were subjected to principal component analysis, and significant components were selected for UMAP clustering. Differentially expressed genes within clusters were identified and validated using ROC curves.

Bulk RNA-seq data (GSE139073) from young (18–44 years) and aged (>65 years) healthy individuals were analyzed. Raw reads were processed using FastQC and aligned with HISAT2. Differential expression was assessed with DESeq, and genes were clustered using k-means. Read counts were normalized to transcripts per million (TPM) for downstream analyses.

Immunofluorescence

Coverslips were placed in six-well plates with a drop of complete medium. A 500 μ L cell suspension was added onto each coverslip and incubated for 4 h. After adding 2 mL of medium, incubation continued overnight. Cells were fixed with 4% paraformaldehyde for 20 min and permeabilized with 0.3% Triton X-100. Following blocking with 5% bovine serum albumin (BSA) at 37 °C for 30 min, cells were incubated overnight at 4 °C with primary antibodies. Secondary antibodies were applied for 1 h at room temperature in the dark. Nuclei were stained with DAPI, and coverslips were mounted using Antifade Mounting Medium (LEAGENE). Fluorescent images were captured via microscopy.

RNA immunoprecipitation (RIP)

RNA immunoprecipitation was conducted using the EZ-Magna RIP Kit (#17–701, Merck Millipore) according to the manufacturer's guidelines. Undifferentiated BMSCs (1×10^7 cells) were lysed and incubated with magnetic beads conjugated to specific antibodies or control IgG overnight at 4 °C. RNA was extracted from immunoprecipitate to assess NEAT1 expression via quantitative real-time PCR (qRT-PCR).

Western blotting

Cells were lysed in RIPA buffer (P0013, Beyotime Biotechnology) containing protease and phosphatase inhibitors. Proteins were separated on 10–15% SDS-PAGE gels and transferred to polyvinylidene difluoride (PVDF) membranes (Merck Millipore). Membranes were blocked with 5% non-fat milk and incubated overnight with primary antibodies (Supplementary Table 1). After washing, membranes were incubated with horseradish peroxidase (HRP)-conjugated secondary antibodies. Bands were visualized using an enhanced chemiluminescence (ECL) kit (Merck Millipore) and quantified with ImageJ software.

Quantitative real-time PCR

Total RNA was extracted using TRIzol reagent. Reverse transcription was performed with the PrimeScript RT reagent kit (Takara Bio). qRT-PCR was carried out using SYBR Green PCR Master Mix (Vazyme) on an ABI Prism 7900 system (Applied Biosystems). Gene expression was normalized to ACTIN, GAPDH, or U1 levels. Experiments were conducted in triplicate, and primer sequences are listed in Supplementary Table 1. The $2^{-\Delta\Delta CT}$ method was used for quantification.

Cytoplasmic/Nuclear separation

Cytoplasmic/Nuclear Separation was performed using the Cytoplasmic/Nuclear Separation Kit (BB-36021, Bestbio) according to the manufacturer's instructions. Briefly, take $5-10 \times 10^6$ cells and centrifuge at 4 °C, 500 \times g for 3 min. Carefully aspirate the medium and collect the cells. Wash the cells twice with cold PBS, draining the supernatant as thoroughly as possible after each wash. Add 400 μ L of cold Extract Solution A to the cell pellet. Swirl or pipette to mix thoroughly, then incubate on ice for 20–30 min with occasional shaking. Centrifuge at 4 °C, 1200 \times g for 5 min. Transfer the supernatant to a pre-chilled clean centrifuge tube to collect the cytoplasmic fraction. Store at 4 °C or use directly for downstream experiments. Wash the pellet with PBS, then centrifuge at 4 °C, 2000 \times g for 5 min. Discard the supernatant. Resuspend the pellet in 200 μ L of Preservation Solution B to isolate the nuclear components. Store for later use or proceed directly with downstream experiments.

Co-immunoprecipitation (Co-IP)

BMSCs were lysed in IP lysis buffer (P0013, Beyotime Biotechnology) with protease and phosphatase inhibitors. Protein lysates (500 μ g) were incubated with 5 μ g of specific antibodies and protein A/G agarose beads (Roche) overnight at 4 °C. Beads were washed, and proteins were eluted for SDS-PAGE analysis. Western blotting was performed using standard protocols and antibodies listed in Supplementary Table 1.

Statistical analysis

Data are presented as mean \pm standard deviation (SD). Experiments were independently replicated at least three times. Statistical significance between two groups was assessed using the student's *t*-test. One-way ANOVA was employed for multiple comparisons, Significance levels were set at **P* < 0.05, ***P* < 0.01, and ****P* < 0.001.

Results

Age-dependent redistribution of NEAT1 from nucleus to cytoplasm

To investigate the role of lncRNA NEAT1 in BMSC aging. Significant age-associated alterations of NEAT1 subcellular localization in bone marrow and BMSCs were observed. Compared with young mice, the number of Nestin⁺ cells were decreased in bone marrow of aged mice, accompanied by significant cytoplasmic localization of fluorescence in situ hybridization (FISH) of NEAT1 (Fig. 1A, Figure S1b-A). Meanwhile, NEAT1 is predominantly confined to the nucleus in young BMSCs (Fig. 1B). In contrast, aged BMSCs exhibited substantial cytoplasmic accumulation of NEAT1, indicating a pronounced shift in subcellular distribution with advancing age (Fig. 1B). Quantitative analysis corroborated this redistribution and we observed that total NEAT1 expression increased significantly with the aging of BMSCs, demonstrating a significant increase in cytoplasmic NEAT1 expression in aged BMSCs (Fig. 1C). Moreover, we used serial passaging as an additional method to induce BMSC aging. Our findings were consistent with previous observations. After 25 generations of continuous passage, BMSCs exhibited distinct morphological signs of senescence (Figure S1b-B). Additionally, the expression level of NEAT1 was significantly increased (Figure S1b-C). Karyoplasmic separation experiments, utilizing actin as a cytoplasmic marker and U1 as a nuclear marker, revealed that NEAT1 progressively translocated from the nucleus to the cytoplasm as BMSCs underwent continuous passage and senescence (Figure S1b-D).

Upon further examination of nuclear division and the post-division stages during BMSCs osteoblasts differentiation, we observed that NEAT1 tightly encircles the nucleus and exhibits a spindle-like polar distribution (Fig. 1D). Additionally, Fluorescence signal analysis suggests that DNA content and NEAT1 expression levels display a positive correlation during karyokinesis, supporting the involvement of NEAT1 in mitosis or cell proliferation (Fig. 1E). These findings suggest that with BMSCs aging, NEAT1 distribution undergoes significant changes, and importantly, its localization is closely associated with nuclear division. Collectively, the results provide valuable insights into NEAT1 potential functional role in cellular aging processes.

NEAT1 related to BMSCs osteoblast differentiation, mitotic cell cycle, and ribosome biogenesis

Given the cytoplasmic localization of NEAT1 associated with aging, NEAT1 knockdown in aged BMSCs led to a reduction in β -glucosidase activity (Fig. 2A). Additionally, we overexpressed NEAT1 in young BMSCs and knocked down NEAT1 in aged BMSCs. We then measured the protein and mRNA levels of senescence-associated secretory phenotype (SASP), including MMP3, IL-6, IL-1 β , and VEGF, as well as classical senescence markers such as p21 and p16. Our results showed that NEAT1 knockdown in aged BMSCs significantly decreased various aging indicators (Fig. 2B and C), while NEAT1 overexpression in young BMSCs led to an increase in these markers (Figure S2A and B). To further elucidate the functional role of NEAT1, RNA pulldown and proteomic analyses were performed to identify its interacting partners in BMSCs. The Venn diagram (Fig. 2D) illustrated the overlap of NEAT1-interacting proteins revealing a core set of 346 conserved proteins. This finding suggests a robust and conserved network of NEAT1-associated proteins indicative of multifaceted functional roles. Proteomic profiling (Fig. 2E) uncovered key proteins enriched within NEAT1 complexes, notably FGF2, which plays a critical role in karyomitosis and cellular proliferation. Other significant interactors included proteins involved in protein nuclear transport, such as Karyopherin Subunit Beta 1 (KPNB1), indicating its broad involvement in cellular processes and protein complex.

Functional enrichment analysis (Fig. 2F) further underscored the biological processes and molecular functions associated with NEAT1-interacting proteins. Top enriched Gene Ontology (GO) terms included protein stabilization, osteoblast differentiation, mitotic cell cycle, and ribosomal biogenesis. The overrepresentation of these proteins emphasizes the essential role of NEAT1 in BMSCs growth, proliferation, and differentiation. These findings suggest that NEAT1 associates with a diverse array of proteins integral to vital cellular processes, particularly within osteogenic pathways.

FGF2 and KPNB1 involves BMSCs proliferation and bone regeneration

Next, the expression patterns of FGF2, KPNB1 during BMSCs proliferation and aging were investigated. Single-cell RNA sequencing data of BMSCs were analyzed using Uniform Manifold Approximation and Projection (UMAP) clustering (Fig. 3A). By delineating the distinct cell populations and their respective cell cycle phases (Fig. 3B) and illustrating the differentiation trajectory of BMSCs (Fig. 3C), potential interactions and transitions between specific cellular states among BMSC clusters were indicated.

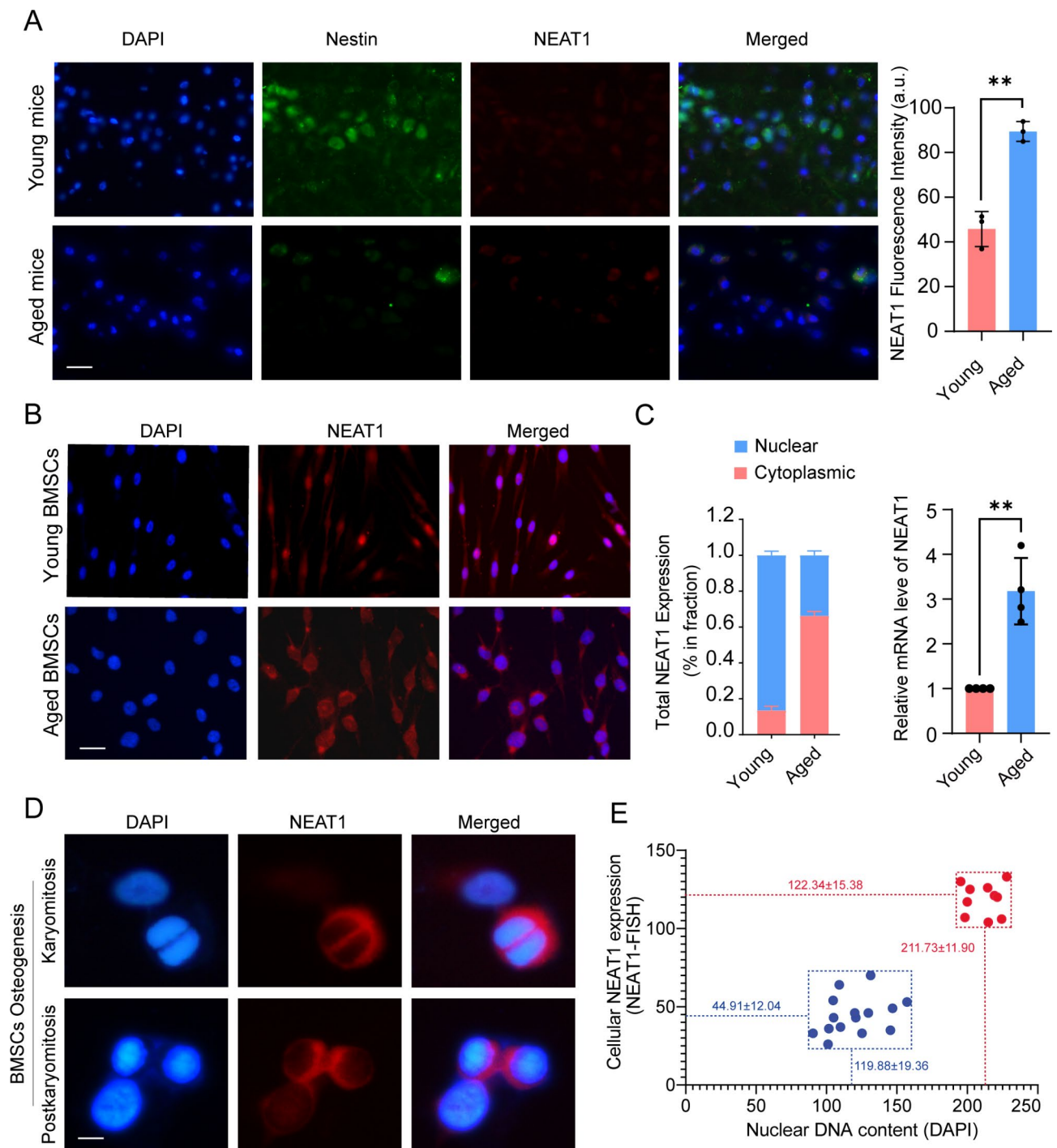


Fig. 1 Age-dependent redistribution of NEAT1 from nucleus to cytoplasm. **(A)** Representative fluorescence images depicting the expression of NEAT1 and Nestin in the bone marrow of young (upper panels) and aged (lower panels) mice. Nuclei are stained with DAPI (blue), immunofluorescence staining of Nestin (green) and FISH staining of NEAT1 (red) are visualized in bone marrow. Scale bar, 40 μ m. **(B)** Representative fluorescence images depicting the subcellular localization of NEAT1 in young (upper panels) and aged (lower panels) BMSCs. Nuclei are stained with DAPI (blue), and NEAT1 is visualized using an RNA-FISH probe (red). Merged images reveal partial cytoplasmic distribution of NEAT1 in aged BMSCs. Scale bar, 20 μ m. **(C)** Quantitative analysis the expression of NEAT1 and localization within nuclear and cytoplasmic compartments in young and aged BMSCs. Data represent mean \pm s.d. **(D)** High-magnification images of NEAT1 localization in individual cells during karyomitosis (top) and postkaryomitosis (bottom). Scale bar, 10 μ m. **(E)** Scatter plot correlating nuclear DNA content (determined by DAPI staining) with cellular NEAT1 expression (quantified by RNA-FISH) during BMSCs osteoblasts differentiation. Data are presented with mean \pm s.d.

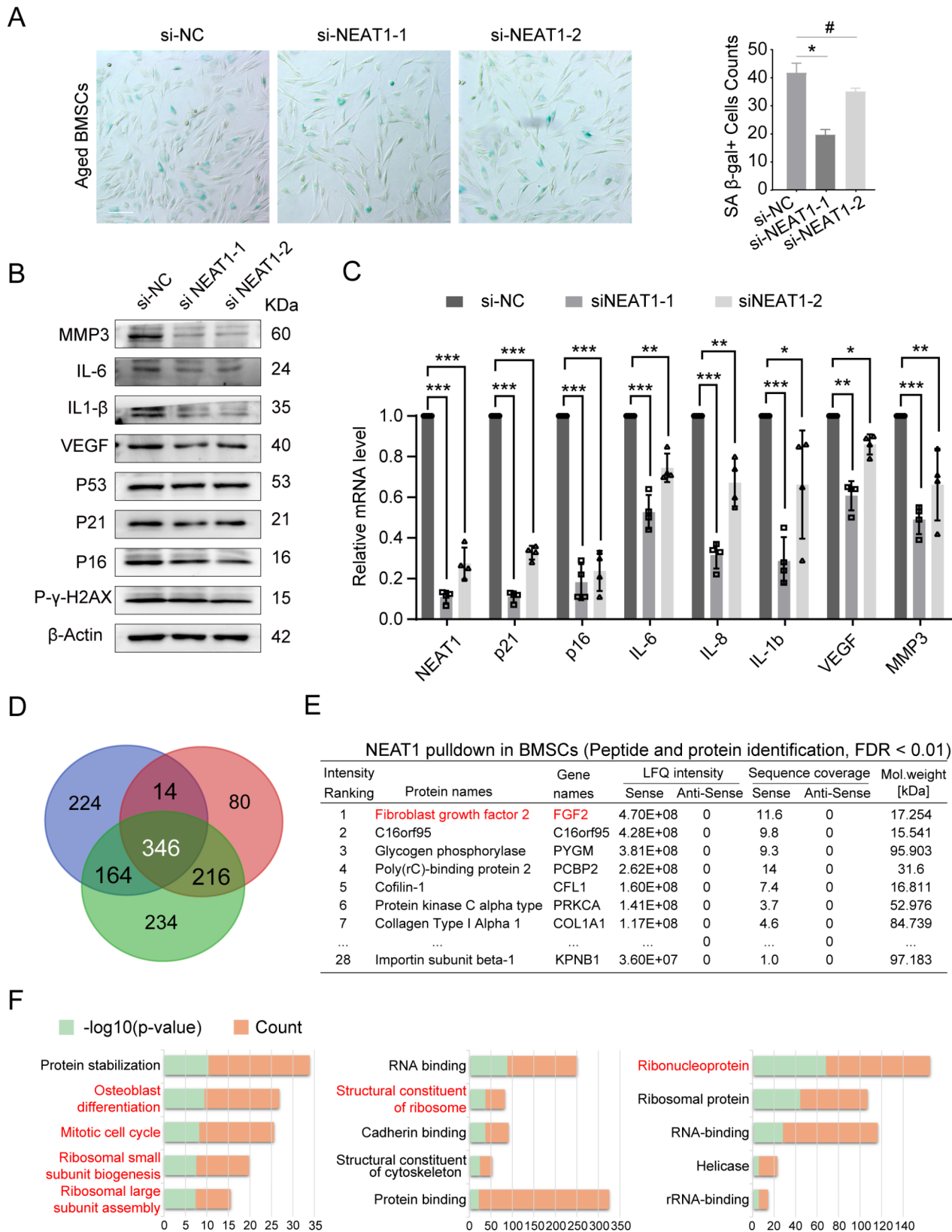


Fig. 2 (See legend on next page.)

(See figure on previous page.)

Fig. 2 NEAT1 related to BMSCs senescence, osteoblast differentiation, mitotic cell cycle, and ribosome biogenesis. **(A)** SA- β -gal staining were applied to aged BMSCs within NEAT1 knockdown, and SA- β -gal positive cells were counted. Scale bar, 40 μ m. **(B)** Western blotting against senescence markers in aged BMSCs following transfection with control siRNA, siNEAT1-1 and siNEAT1-2. Full-length blots are presented in Supplementary Material. **(C)** RT-qPCR analysis of senescence markers in aged BMSCs after transfection with control siRNA, siNEAT1-1 and siNEAT1-2. **(D)** Venn diagram depicting the overlap of NEAT1-interacting proteins identified by mass spectrometry following NEAT1 pulldown experiments in BMSCs. **(E)** List of top-ranked NEAT1-bound proteins in BMSCs based on label-free quantification (LFQ) intensity and peptide coverage, with a false discovery rate (FDR) < 0.01. **(F)** Gene Ontology (GO) term enrichment analysis of NEAT1-associated proteins in BMSCs, categorized by biological processes (left), molecular functions (middle), and cellular component (right)

Gene expression mapping (Fig. 3D and E) revealed the spatial distribution of FGF2, KPNB1, CCND1, and PCNA across cell clusters, with FGF2, KPNB1, and PCNA exhibiting higher expression in proliferative clusters, whereas CCND1 was more uniformly expressed. Quantitative PCR analysis (Fig. 3F) demonstrated that the mRNA levels of FGF2 and KPNB1 were decreased in aged BMSCs compared to young cells. Immunofluorescence staining (Fig. 3G) confirmed the colocalization of FGF2 and KPNB1 within the nuclear compartment of BMSCs.

We next validated our hypothesis in an animal model. Histological analysis of regenerated alveolar bone (Fig. 3I) demonstrated the presence of FGF2 and KPNB1 within the newly formed bone matrix, suggesting their involvement in bone regeneration processes. Moreover, a significant increase in femoral bone thickness was observed following NEAT1 knockdown (Figure S3 A). Key bone parameters such as bone volume fraction (BV/TV), trabecular number (Tb.N), and trabecular thickness (Tb.Th) were all notably improved (Figure S3B). Additionally, H&E and Masson staining revealed that NEAT1 knockdown led to a significant increase in femoral bone content (see Figure S3C and D), suggesting that the NEAT1-FGF2 network plays a critical role in regulating bone regeneration.

The region of FGF2 that binds to NEAT1 is enriched with nuclear localization motifs

To explore the molecular mechanisms underlying NEAT1 related regulatory effects, its interaction with FGF2 and KPNB1 was examined. The NEAT1-FGF2 interaction matrix identified specific residues within FGF2, that strongly associate with particular NEAT1 nucleotide regions, suggesting sequence-specific binding (Fig. 4A). The NLS Mapper (<http://nls-mapper.iab.keio.ac.jp/>) and NetworKIN (<http://networkin.info/>) further indicated the region of FGF2 that binds to NEAT1 is enriched with nuclear localization signal (NLS) motif (Fig. 4B). This suggests that the specific binding of NEAT1 may play a potential role in influencing FGF2 nuclear translocation.

Consistent with the mass spectrometry, RNA pulldown assays demonstrated that NEAT1 in BMSCs resulted in specific enrichment of the 18-kDa FGF2 isoform and KPNB1, confirming the specificity of the NEAT1/FGF2/KPNB1 interactions (Fig. 4C). RNA immunoprecipitation

(RIP) assays (Fig. 4D) further confirmed significant enrichment of NEAT1 bound to FGF2 in BMSCs, reinforcing the specificity and strength of their interaction. Moreover, a significant increase in FGF2 nuclear accumulation in aged mouse BMSCs were observed after NEAT1 knockdown (Fig. 4E). These findings reveal that NEAT1 exerts a critical regulatory influence on FGF2, likely modulating its transport and function through molecular complex, and potentially impacting cellular processes such as nuclear import and BMSCs proliferation.

NEAT1 reduces interaction between FGF2 and KPNB1

To assess the regulatory effects of NEAT1 on FGF2 & KPNB1 interactions and FGF2 nuclear transport, knockdown and overexpression experiments were performed in aged BMSCs and young BMSCs, respectively. Compared to the effects of NEAT1 knockdown (Fig. 5A) and overexpression (Fig. 5B) on the global expression levels of FGF2, co-immunoprecipitation indicates that after NEAT1 knockdown, KPNB1 binds more FGF2, promoting the nuclear transport of FGF2 (Fig. 5C). Conversely, when NEAT1 is overexpressed, it binds to the nuclear localization motif of FGF2, affecting FGF2 binding to KPNB1 and FGF2 nuclear transport (Fig. 5D).

Co-immunoprecipitation and mass spectrum analyses (Fig. 5E) further highlighted key biological processes and pathways influenced by FGF2. Top enriched GO terms included positive regulation of myoblast differentiation, mitotic spindle assembly checkpoint signaling, regulation of microtubule nucleation, translation, and RNA binding, while Kyoto Encyclopedia of Genes and Genomes (KEGG) pathways revealed significant enrichment in nucleocytoplasmic transport, DNA replication, and signaling pathways regulating stem cell pluripotency. These results suggest that NEAT1/FGF2-associated protein complexes participate in critical cellular processes linked to cell differentiation and proliferation.

Discussion

Aging significantly impairs the proliferative and regenerative capacity of BMSCs, which is essential for maintaining bone homeostasis and facilitating bone repair [28, 29]. As a critical nuclear-paraspeckle component, NEAT1 has emerged involved in gene expression regulation, cellular proliferation and senescence [30–33]. Concurrently, as the growth factor of BMSCs, fibroblast

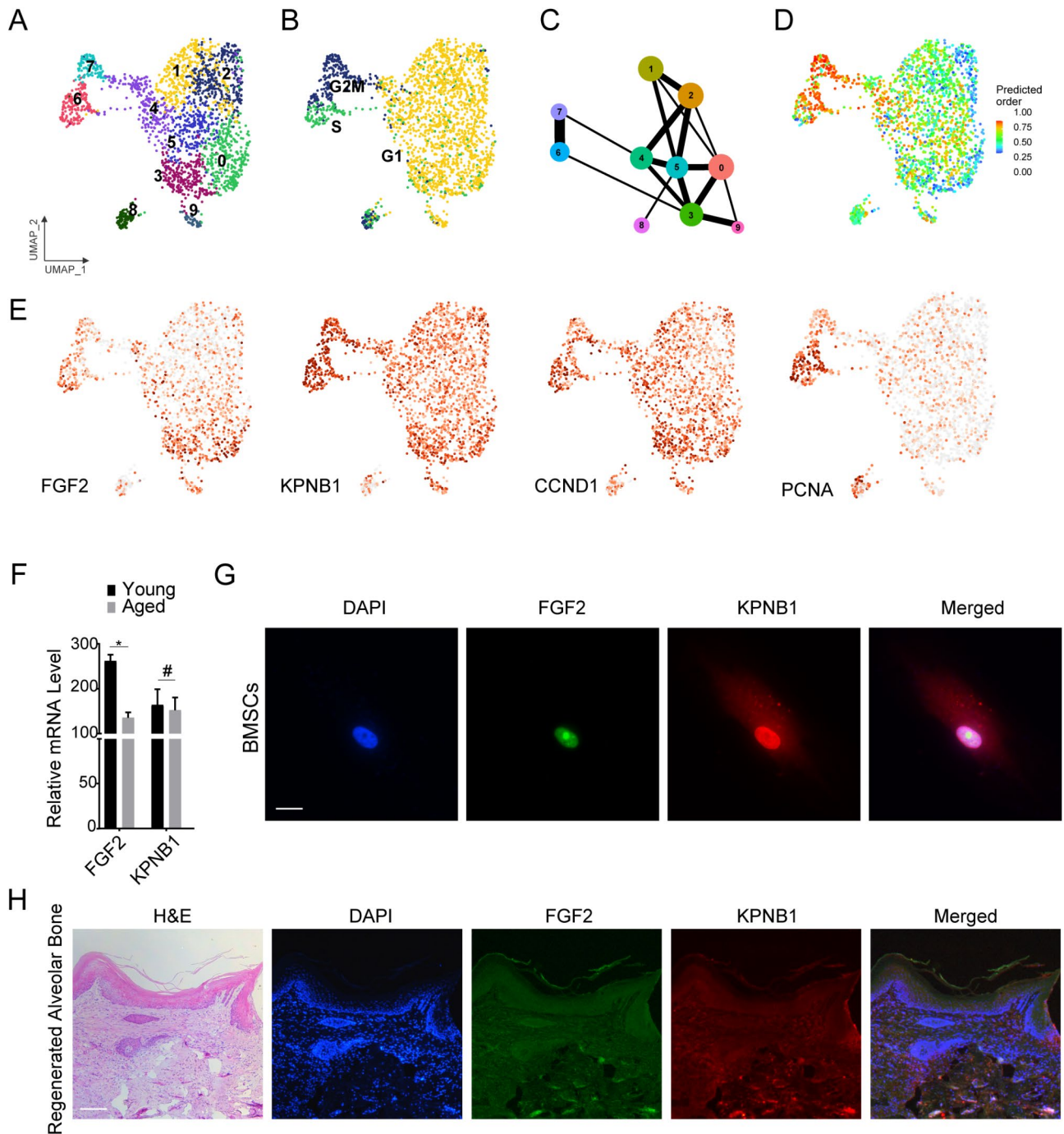


Fig. 3 FGF2 and KPNB1 involves in BMSCs proliferation and bone regeneration. **(A)** Uniform Manifold Approximation and Projection (UMAP) plot illustrating distinct clusters of BMSCs, based on single-cell RNA sequencing data. Clusters are numbered and color-coded, reflecting heterogeneity within the BMSC population. **(B)** UMAP projection of BMSC cell cycle states, displaying cells in G1, S, and G2/M phases. The majority of cells reside in the G1 phase, with smaller subsets in the S and G2/M phases, indicating proliferative diversity within the population. **(C)** Partition-based graph abstraction (PAGA) was used to analyze and visualize cellular differentiation trajectories. **(D-E)** Expression density plots visualizing the distribution of FGF2, KPNB1, CCND1, and PCNA transcripts across BMSC populations. **(F)** RT-qPCR analysis of FGF2 and KPNB1 expression levels in young and aged BMSCs. Expression levels of FGF2 are upregulated in young BMSCs (* $P < 0.05$). Data represent mean \pm s.d. **(G)** Immunofluorescence staining of FGF2 (green) and KPNB1 (red) in cultured BMSCs. Nuclei are counterstained with DAPI (blue). Merged images reveal colocalization of FGF2 and KPNB1 within the nuclear compartment. Scale bar, 10 μ m. **(H)** Histological analysis of regenerated alveolar bone from mice. Hematoxylin and eosin (H&E) staining highlights bone regeneration morphology, whereas immunofluorescence staining demonstrates the presence of FGF2 (green) and KPNB1 (red) within the newly formed bone matrix. Nuclei are counterstained with DAPI (blue), and merged images show the spatial localization of FGF2 and KPNB1. Scale bar, 50 μ m

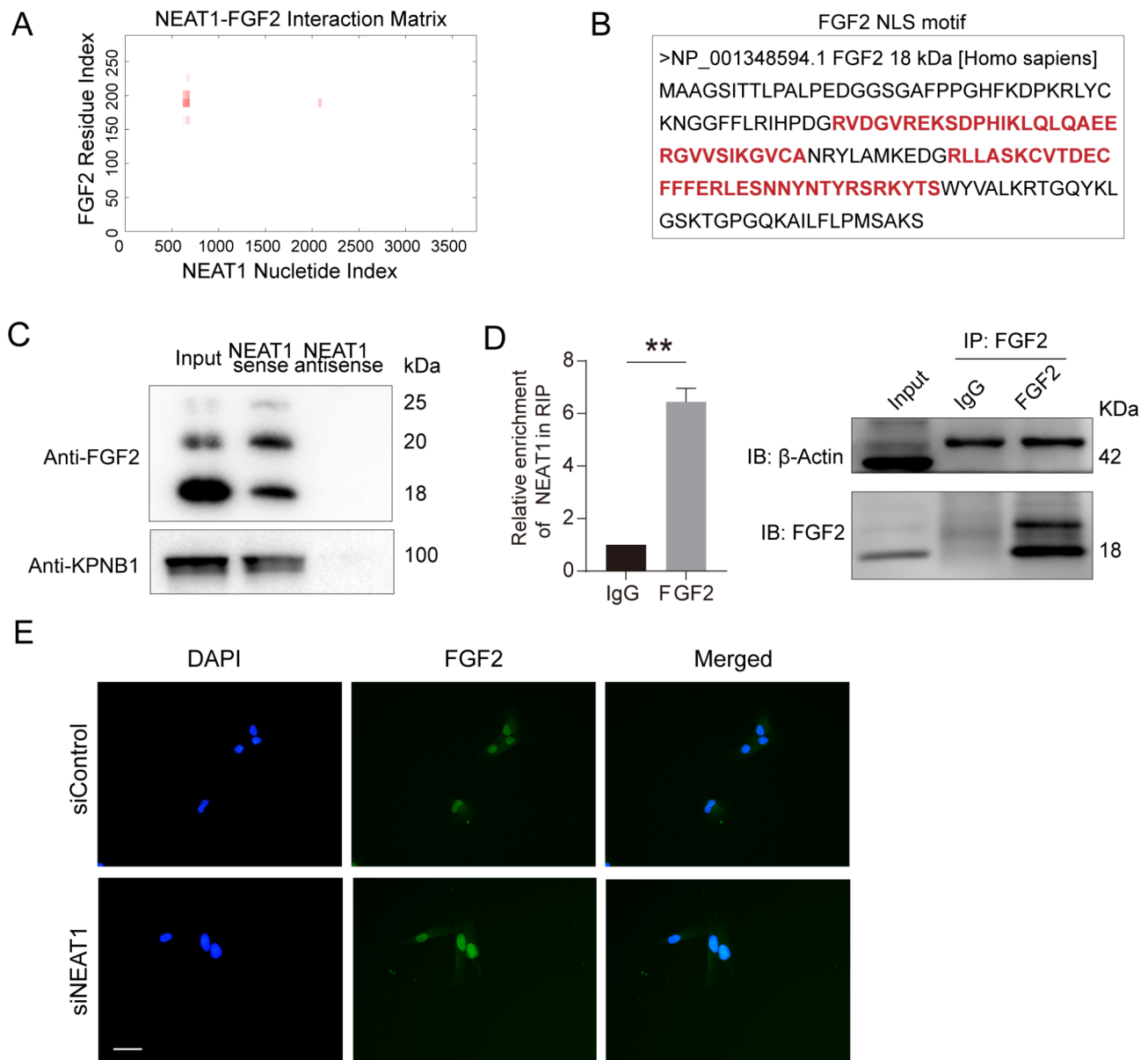


Fig. 4 The region of FGF2 that binds to NEAT1 is enriched with nuclear localization motifs. **(A)** The NEAT1–FGF2 interaction matrix identifies specific regions within FGF2, that strongly associate with particular NEAT1 nucleotide regions, suggesting sequence-specific binding between NEAT1 and FGF2. **(B)** Sequence alignment of the FGF2 nuclear localization signal (NLS) motif. The 18-kDa FGF2 protein sequence (NP_001348594.1) highlights conserved residues critical for nuclear import. Key positively charged and hydrophobic residues are indicated in red, delineating the NLS domain essential for FGF2 nuclear translocation and interaction with NEAT1. **(C)** NEAT1 sense and antisense pulldown assays demonstrate specific enrichment of the 18-kDa FGF2 isoform and KPNB1 in BMSCs. **(D)** RNA immunoprecipitation (RIP) assay showing significant enrichment of NEAT1 bound to 18-kDa FGF2 in BMSCs (** $P < 0.01$). Data are presented as mean \pm s.d. Full-length blots are presented in Supplementary Material. **(E)** Immunofluorescence staining of FGF2 (green) in cultured aged mouse BMSCs after transfection with control siRNA and siNEAT1. Nuclei are counterstained with DAPI (blue). Scale bar, 20 μ m

growth factors are well-documented for the mitogenic roles in involving cellular growth, proliferation, and differentiation [18, 19]. Despite their individual importance, the interplay between NEAT1 and FGF2 in the context of BMSCs aging and differentiation remains insufficiently explored. In this study, we discovered that NEAT1 undergoes age-dependent subcellular redistribution in BMSCs, interacts with FGF2 and KPNB1, and modulates FGF2

nuclear localization, thereby influencing BMSCs proliferation and osteogenic differentiation.

NEAT1 is a nuclear-enriched abundant transcript, has been extensively studied for its role in paraspeckle formation and regulation of gene expression during the cell cycle [33, 34]. Previous research implicated NEAT1 in maintaining nuclear integrity, modulating transcriptional activity, and influencing cellular senescence and

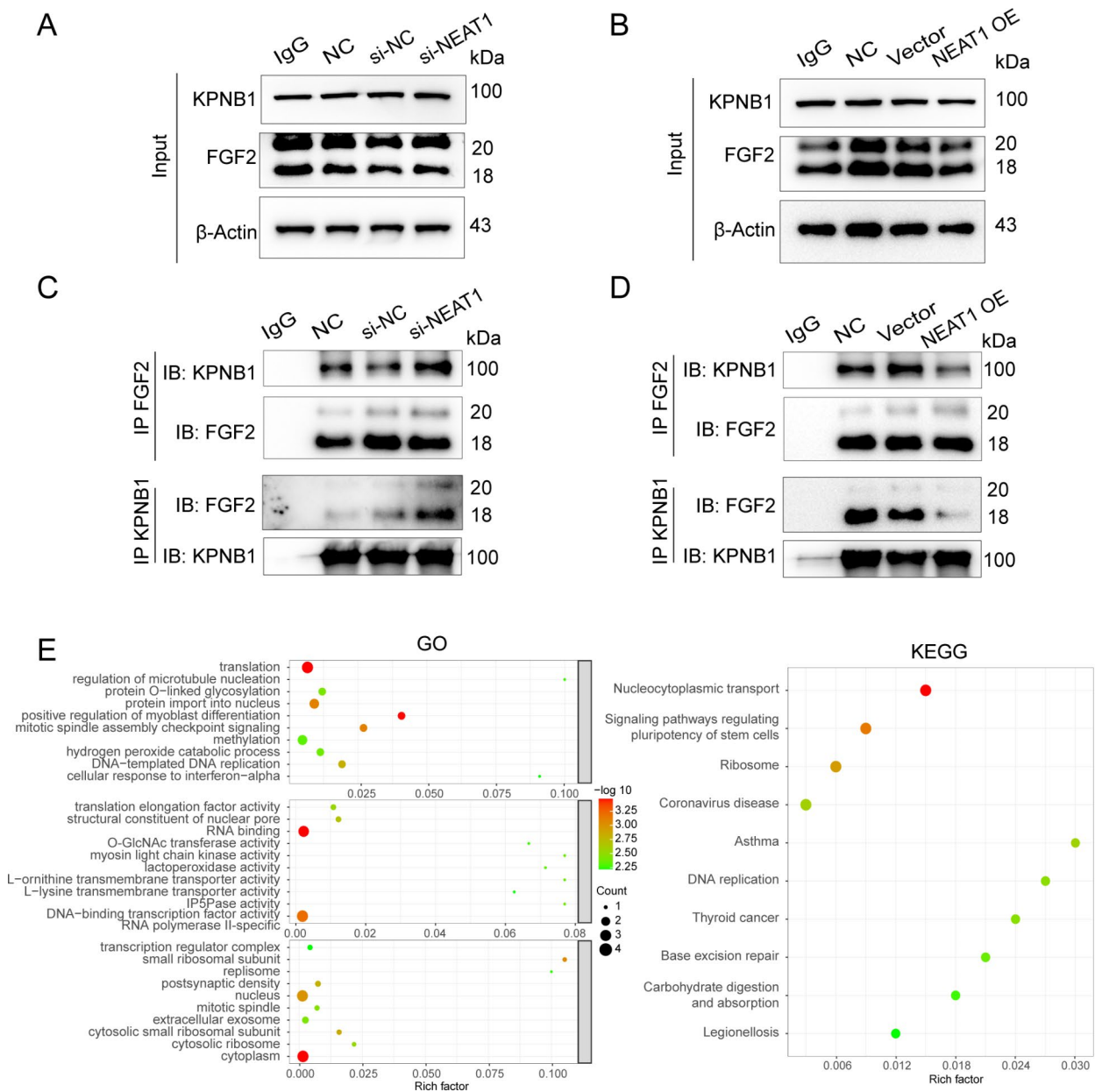


Fig. 5 NEAT1 reduces interaction between FGF2 and KPNB1. **(A-B)** Immunoblot analysis of FGF2 expression in aged BMSCs following NEAT1 knockdown and young BMSCs following NEAT1 overexpressing, respectively. Full-length blots are presented in Supplementary Material. **(C)** Co-immunoprecipitation (co-IP) of FGF2 and KPNB1 from BMSCs with or without NEAT1 knockdown. Full-length blots are presented in Supplementary Material. **(D)** Co-immunoprecipitation of FGF2 and KPNB1 from NEAT1-overexpressing BMSCs. Full-length blots are presented in Supplementary Material. **(E)** Gene Ontology (GO) (left) and Kyoto Encyclopedia of Genes and Genomes (KEGG) (right) enrichment analyses of FGF2-interacting proteins, highlighting key biological processes and pathways influenced by FGF2

differentiation [35, 36]. Importantly, the increased cytoplasmic accumulation of NEAT1 involved mRNA stability and related signaling pathways [15]. Meanwhile, aligns with previous research [37] the correlation between elevated expression levels and increased nuclear DNA content implies the relationship between NEAT1 and cell proliferation. In this study, the observed age-dependent redistribution of NEAT1 from the nucleus to the cytoplasm in BMSCs correlates with diminished proliferative

capacity, underscoring the functional significance of its subcellular localization. Moreover, during BMSCs differentiation, NEAT1 binds with abundant mitogenic FGF2, encircles the nucleus, and exhibits spindle-like distribution of polarity, suggesting its involvement in cell proliferation regulation. This interaction reveals that NEAT1 influences BMSCs homeostasis by modulating FGF2 activity, integrating previous insights on NEAT1 regulatory roles with its impact on BMSC aging processes.

Nuclear localization signals (NLSs) are specific short amino acid sequences, which directed proteins to the nucleus by facilitating their recognition by karyopherin [38]. These specific motifs are essential for the protein nuclear import and performing critical functions. In this study, as well as binding to FGF2 and KPNB1, NEAT1 specifically binds to the NLS region of FGF2, which suggests a novel competitive mechanism wherein NEAT1 may inhibit the interaction between FGF2 and KPNB1 by occupying FGF2 NLS region. Consequently, NEAT1 overexpression reduces FGF2-KPNB1 binding, hindering FGF2 nuclear translocation and impairing BMSC proliferation and osteogenic differentiation. Conversely, NEAT1 knockdown enhances FGF2-KPNB1 interaction and promotes nuclear import of FGF2, thereby facilitating proliferation and differentiation. Meanwhile, NEAT1 pulldown analyses validated that NEAT1 interacts with a diverse array of proteins involved in mitotic cell cycle, ribosome biogenesis, cytoskeletal organization, and osteoblast differentiation. The enrichment of ribosomal proteins and cyclins among NEAT1 interactors underscores its potential role in cell growth and differentiation [39]. This mechanism resembles that NEAT1 acting as molecular scaffolds, particularly relevant in aging, where the maintenance of efficient signaling networks is crucial for cellular function [35, 36].

Conclusions

Our findings provide significant insights into the control of FGF2 nuclear transport processes by NEAT1, which underscores a pivotal regulatory axis that influences BMSCs aging, offering potential avenues for therapeutic intervention in age-related bone disorders.

Supplementary Information

The online version contains supplementary material available at <https://doi.org/10.1186/s13287-025-04156-1>.

Supplementary Material 1

Supplementary Material 2

Supplementary Material 3

Acknowledgements

We thanked Yi Zhang for providing technical assistance in single-cell RNA-Seq analysis.

Author contributions

Conceptualization, H.Z. and J.X.; methodology, Z.W., H.Z., and Wenyu Zhen.; software, Wenyu Zhen, Q.W., and Y.S.; formal analysis, Z.W., S.J., S.Y., and X.W.; investigation, Z.W., Q.W., Wenhao Zhang, Y.Z., F.X., R.W. and Y.X.; resources, H.Z., W.S., and Z.W.; writing original draft, H.Z., Z.W., and Wenyu Zhen; writing review & editing, all authors; visualization, Z.W., W.S., and Q.W.; supervision, H.Z., J.X. and W.S.; funding acquisition, H.Z., J.X. and W.S.

Funding

This research was funded by grants from the National Natural Science Foundation of China (no. 82201026), Natural Science Foundation of Anhui Province (no. 2408085MH221), Outstanding Young Teacher

Development Program for Higher Education Institutions of Anhui Province (no. YQYB2024013), the School Foundation of Anhui Medical University (no. 2023xkj041), Anhui Medical University Student Innovation and Entrepreneurship Training Program (no. S202410366087 and S202410366086).

Data availability

The accession numbers for the Single Cell RNA-seq and RNA-seq data reported in this paper are Gene Expression Omnibus (GEO): GSE113253, GSE139073. Mass spectrometric data were uploaded at iProX (Project ID: IPX0010879000).

Declarations

Ethical approval and consent to participate

This study was performed in line with the principles of the Declaration of Helsinki, and written informed consent was obtained from all individual participants before being enrolled in the study. The study design, protocol and informed consent were approved and adopted by the Ethical Committee at Anhui Medical University and the College & Hospital of Stomatology of Anhui Medical University. The project "Collecting jaw bone fragments during dental implant surgery to prepare primary human bone marrow mesenchymal stem cells" was approved on October 20, 2021 with approval number of T2021014. The project "Animal study on the mechanism of aging jaw bone and related BMSCs" was approved on May 30, 2023 with approval number of LLSC20232087.

Consent for publication

Not applicable.

Competing interests

All authors declare no competing interests. All co-authors have seen and agreed with the contents of the manuscript and there is no financial interest to report.

Author details

¹College & Hospital of Stomatology, Key Laboratory of Oral Diseases Research of Anhui Province, Anhui Medical University, Hefei 230032, China

²Department of Stomatology, The First Affiliated Hospital of Anhui Medical University, Hefei 230032, China

Received: 31 October 2024 / Accepted: 21 January 2025

Published online: 29 January 2025

References

1. López-Otin C, Blasco MA, Partridge L, Serrano M, Kroemer G. Hallmarks of aging: an expanding universe. *Cell*. 2023;186(2):243–78.
2. Campisi J, Kapahi P, Lithgow GJ, Melov S, Newman JC, Verdin E. From discoveries in ageing research to therapeutics for healthy ageing. *Nature*. 2019;571(7764):183–92.
3. Hou Y, Dan X, Babbar M, Wei Y, Hasselbalch SG, Croteau DL, Bohr VA. Ageing as a risk factor for neurodegenerative disease. *Nat Rev Neurol*. 2019;15(10):565–81.
4. Pittenger MF, Discher DE, Peault BM, Phinney DG, Hare JM, Caplan AI. Mesenchymal stem cell perspective: cell biology to clinical progress. *NPJ Regen Med*. 2019;4:22.
5. Lin H, Sohn J, Shen H, Langhans MT, Tuan RS. Bone marrow mesenchymal stem cells: aging and tissue engineering applications to enhance bone healing. *Biomaterials*. 2019;203:96–110.
6. Ambrosi TH, Scialdone A, Graja A, Gohlke S, Jank AM, Bocian C, Woelk L, Fan H, Logan DW, Schurmann A, et al. Adipocyte accumulation in the bone marrow during obesity and aging impairs stem cell-based hematopoietic and bone regeneration. *Cell Stem Cell*. 2017;20(6):771–e784776.
7. Zupan J, Strazar K, Kocijan R, Nau T, Grillari J, Marolt Presen D. Age-related alterations and senescence of mesenchymal stromal cells: implications for regenerative treatments of bones and joints. *Mech Ageing Dev*. 2021;198:111539.
8. Mercer TR, Dingler ME, Mattick JS. Long non-coding RNAs: insights into functions. *Nat Rev Genet*. 2009;10(3):155–9.

9. Statello L, Guo CJ, Chen LL, Huarte M. Gene regulation by long non-coding RNAs and its biological functions. *Nat Rev Mol Cell Biol.* 2021;22(2):96–118.
10. Kopp F, Mendell JT. Functional classification and experimental dissection of long noncoding RNAs. *Cell.* 2018;172(3):393–407.
11. Hirose T, Yamazaki T, Nakagawa S. Molecular anatomy of the architectural NEAT1 noncoding RNA: the domains, interactors, and biogenesis pathway required to build phase-separated nuclear paraspeckles. *Wiley Interdisciplinary Reviews RNA.* 2019;10(6):e1545.
12. Yamazaki T, Souquere S, Chujo T, Kobelke S, Chong YS, Fox AH, Bond CS, Nakagawa S, Pierron G, Hirose T. Functional domains of NEAT1 architectural lncRNA induce paraspeckle assembly through phase separation. *Mol Cell.* 2018;70(6):1038–e1031037.
13. Clemson CM, Hutchinson JN, Sara SA, Ensminger AW, Fox AH, Chess A, Lawrence JB. An architectural role for a nuclear noncoding RNA: NEAT1 RNA is essential for the structure of paraspeckles. *Mol Cell.* 2009;33(6):717–26.
14. Li K, Wang Z. lncRNA NEAT1: key player in neurodegenerative diseases. *Ageing Res Rev.* 2023;86:101878.
15. Zhang H, Xu R, Li B, Xin Z, Ling Z, Zhu W, Li X, Zhang P, Fu Y, Chen J, et al. lncRNA NEAT1 controls the lineage fates of BMSCs during skeletal aging by impairing mitochondrial function and pluripotency maintenance. *Cell Death Differ.* 2022;29(2):351–65.
16. Wen S, Wei Y, Zen C, Xiong W, Niu Y, Zhao Y. Long non-coding RNA NEAT1 promotes bone metastasis of prostate cancer through N6-methyladenosine. *Mol Cancer.* 2020;19(1):171.
17. Zhao M, Liu S, Wang Y, Lv K, Lou P, Zhou P, Zhu J, Li L, Cheng J, Lu Y, et al. The mitochondria–paraspeckle axis regulates the survival of transplanted stem cells under oxidative stress conditions. *Theranostics.* 2024;14(4):1517–33.
18. Ornitz DM, Itoh N. The fibroblast growth factor signaling pathway. *Wiley Interdiscip Rev Dev Biol.* 2015;4(3):215–66.
19. Turner N, Grose R. Fibroblast growth factor signalling: from development to cancer. *Nat Rev Cancer.* 2010;10(2):116–29.
20. Li HZ, Zhang JL, Yuan DL, Xie WQ, Ladel CH, Mobasheri A, Li YS. Role of signaling pathways in age-related orthopedic diseases: focus on the fibroblast growth factor family. *Military Med Res.* 2024;11(1):40.
21. Chen L, Carlton M, Chen X, Kaur N, Ryan H, Parker TJ, Lin Z, Xiao Y, Zhou Y. Effect of fibronectin, FGF-2, and BMP4 in the stemness maintenance of BMSCs and the metabolic and proteomic cues involved. *Stem Cell Res Ther.* 2021;12(1):165.
22. Li Q, Liu T, Zhang L, Liu Y, Zhang W, Liu W, Cao Y, Zhou G. The role of bFGF in down-regulating alpha-SMA expression of chondrogenically induced BMSCs and preventing the shrinkage of BMSC engineered cartilage. *Biomaterials.* 2011;32(21):4773–81.
23. Xiao L, Liu P, Li X, Doetschman T, Coffin JD, Drissi H, Hurley MM. Exported 18-kDa isoform of fibroblast growth factor-2 is a critical determinant of bone mass in mice. *J Biol Chem.* 2009;284(5):3170–82.
24. Kimura M, Imamoto N. Biological significance of the importin-beta family-dependent nucleocytoplasmic transport pathways. *Traffic.* 2014;15(7):727–48.
25. Soniat M, Chook YM. Karyopherin-beta2 recognition of a PY-NLS variant that lacks the proline-tyrosine motif. *Structure.* 2016;24(10):1802–9.
26. Zhen Y, Sorensen V, Skjærpen CS, Haugsten EM, Jin Y, Walchli S, Olsnes S, Wiedlocha A. Nuclear import of exogenous FGF1 requires the ER-protein LRRC59 and the importins Kpnalpha1 and Kpnbeta1. *Traffic.* 2012;13(5):650–64.
27. Hurt E, Beck M. Towards understanding nuclear pore complex architecture and dynamics in the age of integrative structural analysis. *Curr Opin Cell Biol.* 2015;34:31–8.
28. Zhou S, Greenberger JS, Epperly MW, Goff JP, Adler C, Leboff MS, Glowacki J. Age-related intrinsic changes in human bone-marrow-derived mesenchymal stem cells and their differentiation to osteoblasts. *Ageing Cell.* 2008;7(3):335–43.
29. Ambrosi TH, Scialdone A, Graja A, Gohlke S, Jank AM, Bocian C, Woelck L, Fan H, Logan DW, Schürmann A, et al. Adipocyte accumulation in the bone marrow during obesity and aging impairs stem cell-based hematopoietic and bone regeneration. *Cell Stem Cell.* 2017;20(6):771–e784776.
30. Xiao P, Zhu X, Sun J, Zhang Y, Qiu W, Li J, Wu X. lncRNA NEAT1 regulates chondrocyte proliferation and apoptosis via targeting miR-543/PLA2G4A axis. *Hum Cell.* 2021;34(1):60–75.
31. Hu X, Li F, He J, Yang J, Jiang Y, Jiang M, Wei D, Chang L, Hejtmanic JF, Hou L, et al. lncRNA NEAT1 recruits SFPO to regulate MITF splicing and control RPE cell proliferation. *Invest Ophthalmol Vis Sci.* 2021;62(14):18.
32. Yang Q, Chen S, Wang X, Yang X, Chen L, Huang T, Zheng Y, Zheng X, Wu X, Sun Y, et al. Exercise mitigates endothelial pyroptosis and atherosclerosis by downregulating NEAT1 through N6-methyladenosine modifications. *Arterioscler Thromb Vasc Biol.* 2023;43(6):910–26.
33. Zhang H, Su X, Burley SK, Zheng XFS. mTOR regulates aerobic glycolysis through NEAT1 and nuclear paraspeckle-mediated mechanism in hepatocellular carcinoma. *Theranostics.* 2022;12(7):3518–33.
34. Adriaens C, Standaert L, Barra J, Latil M, Verfaillie A, Kalev P, Boeckx B, Wijnhoven PW, Radaelli E, Vermi W, et al. p53 induces formation of NEAT1 lncRNA-containing paraspeckles that modulate replication stress response and chemosensitivity. *Nat Med.* 2016;22(8):861–8.
35. Chakravarty D, Sboner A, Nair SS, Giannopoulou E, Li R, Hennig S, Mosquera JM, Pauwels J, Park K, Kossai M, et al. The oestrogen receptor alpha-regulated lncRNA NEAT1 is a critical modulator of prostate cancer. *Nat Commun.* 2014;5:5383.
36. Wang Y, Hu SB, Wang MR, Yao RW, Wu D, Yang L, Chen LL. Genome-wide screening of NEAT1 regulators reveals cross-regulation between paraspeckles and mitochondria. *Nat Cell Biol.* 2018;20(10):1145–58.
37. Luo OJ, Lei W, Zhu G, Ren Z, Xu Y, Xiao C, Zhang H, Cai J, Luo Z, Gao L, et al. Multidimensional single-cell analysis of human peripheral blood reveals characteristic features of the immune system landscape in aging and frailty. *Nat Aging.* 2022;2(4):348–64.
38. Lu J, Wu T, Zhang B, Liu S, Song W, Qiao J, Ruan H. Types of nuclear localization signals and mechanisms of protein import into the nucleus. *Cell Commun Signal.* 2021;19(1):60.
39. Kofler L, Grundmann L, Gerhalter M, Prattes M, Merl-Pham J, Zisser G, Grishkovskaya I, Hodirnau VV, Vareka M, Breinbauer R, et al. The novel ribosome biogenesis inhibitor usnic acid blocks nucleolar pre-60S maturation. *Nat Commun.* 2024;15(1):7511.

Publisher's note

Springer Nature remains neutral with regard to jurisdictional claims in published maps and institutional affiliations.